Iterative Reconstruction of Medical Ultrasound Images Using Spectrally Constrained Phase Updates

Oleg Michailovich, Adrian Basarab, Denis Kouamé

ITERATIVE RECONSTRUCTION OF MEDICAL ULTRASOUND IMAGES USING SPECTRALLY CONSTRAINED PHASE UPDATES

Oleg Michailovich[⋆] *Adrian Basarab*[†] *Denis Kouame*[†]

[⋆] Department of Electrical and Computer Engineering, University of Waterloo, Canada
[†] Informatics Research Institute of Toulouse, Paul Sabatier University (Toulouse III), France

ABSTRACT

Image deconvolution is a standard numerical procedure used in medical ultrasound imaging for improving the resolution and contrast of diagnostic sonograms. However, due to the intrinsic bandlimitedness of ultrasound scanners and the adverse effect of measurement noises, image deconvolution is known to be exceedingly sensitive to the errors incurred during inference of the point spread function (PSF) that characterizes the imaging system in use. In this case, even the slightest errors in specification of the PSF are likely to result in significant artifacts, rendering the reconstructed images worthless. To address the aforementioned problem, this paper describes a new method for blind deconvolution of ultrasound images, in which the errors due to inaccuracies in specification of the PSF are eliminated concurrently with estimation of tissue reflectivity directly from its associated radio-frequency data. A principal derivation and justification of the proposed method are supported by experimental results which demonstrate the effectiveness and viability of the new technique.

Index Terms— Medical ultrasound, blind deconvolution, alternating minimization, all-pass filtering.

1. INTRODUCTION

The last few decades have witnessed significant developments in medical ultrasound technology, which nowadays features a wide spectrum of devices, ranging from high-end clinical sonographs to lightweight pocket-sized scanners particularly optimized for point-of-care application. Without doubt, the operational means of implementation of ultrasound imaging will continue their advance for many years to come, bringing about faster scanners with progressively improving functionality. This being said, however, the physical principles of ultrasound imaging harbour some principal limitations which seem to be impossible to rectify through the sophistication of hardware design alone. In particular, the intrinsic bandlimitedness of ultrasound scanners along with the coherent nature of ultrasound image formation remain responsible for the familiar limitations of this imaging modality in terms of its effective spatial resolution and contrast. These limitations, on the other hand, can be alleviated by post-processing means, among which image deconvolution is arguably the most traditional method of choice [1].

In medical ultrasound imaging, adopting the convolution model of image formation requires one to exercise some precautions, since, strictly speaking, this model can only be applied under certain assumptions, collectively known as the first Born approximation [2]. Even though the conditions of this approximation are nearly met in soft biological tissues, applying the convolution model to an entire image is rarely advised in view of the spatial variability of the PSF. Indeed, more often than not, the effect of dispersive attenuation along with the non-uniformity of acoustic focusing make the PSF vary across the image domain [3]. This being said, however, the above variability has been observed to be relatively slow in most practical scenarios, which makes it possible to apply the convolution model to localized segments of an ultrasound scan[1]. For this reason, the discussion below will be restricted to one of such segments, associated with a spatially invariable, yet generally unknown PSF.

In medical ultrasound, the problem of blind deconvolution – deconvolution with an unknown PSF – has been addressed through a variety of different methods. In their majority, these methods can be divided into two general subgroups, depending on the way the uncertainty in the definition of PSF is dealt with. Specifically, one approach is to recover an estimate of the PSF first, followed by image reconstruction by means of "non-blind" deconvolution [4, 5]. Such methods frequently offer the possibility of fast implementation, accompanied by some credible convergence guarantees. On the downside, the methods usually depend on somewhat strict assumptions on the nature of the PSF, which has a negative effect on the range of their practical applicability. In contrast, an alternative approach aims at recovering the PSF concurrently with the process of image reconstruction [6]. While considerably more general in comparison to the previous subgroup of approaches, these methods usually come with weaker guaranties of convergence to globally optimal solutions, which undermines their value for diagnostic applications.

In an attempt to consolidate the strong features of the two

[1] Partitioning the entire image domain into 3-4 sectors along the axial and lateral directions usually works well for most commercial scanners in both cardiac and abdominal settings.

methodologies mentioned above, a "hybrid" approach to the problem of blind deconvolution was discussed in [7]. The key idea underlying this approach is to deconvolve ultrasound images using only partial information about the PSF, such as, for instance, its power spectrum. The "hybrid" algorithm was derived based on an explicit formulation, aiming at estimation of an optimal inverse filter, whose application to the data image would yield the desired reconstruction. The results produced by the "hybrid" deconvolution have been demonstrated to match closely those of Wiener filtering. However, similarly to the latter case, the linearity of inverse filtering always confines its action to the scanner's passband, taking its toll on the quality of image reconstruction in terms of residual blur and Gibb's like artifacts.

The main goal of this work has been to alleviate the aforementioned drawback of "hybrid" deconvolution through its formulation as an implicit inverse problem. We show that the proposed method leads to solution of a familiar reconstruction problem, augmented with an analytical update of the spectral phase of the PSF. The effectiveness and practical value of the new method are demonstrated through experiments with real-life data.

2. PROPOSED METHODOLOGY

As usual, we begin with establishing some necessary nomenclature and notations, starting with an image formation model of the form

$$g = f * h + \eta, \tag{1}$$

where g denotes an $N \times M$ (quasi-)stationary segment of a radio-frequency (RF) image contaminated by a noise term η, while h and f stand for the PSF and tissue reflectivity function associated with the given segment, respectively. Note that model (1) can be equally applied to in-phase/quadrature (IQ) data, which might offer a substantial reduction in the number of computations due to subsampling (albeit at the expense of complex arithmetics). In this work, both analytical derivations and data processing were carried out in the IQ domain, with appropriate interpretation of the variables in (1).

In blind deconvolution, only the measured data g is assumed to be known, with both f and h treated as unknowns. However, it is usually possible to make some reasonable assumptions regarding either the functional or statistical nature of the latter. Such assumptions are usually "encoded" in the action of properly defined real-valued functionals φ and ψ which attain relatively small values for all admissible f and h, correspondingly. In this case, the problem of blind deconvolution can be formulated as an optimization problem of the form

$$\min_{f,h} \left\{ (1/2) \left\| f * h - g \right\|_F^2 + \varphi(f) + \psi(h) \right\}, \tag{2}$$

with $\|\cdot\|_F$ denoting the Frobenius matrix norm. Subsequently, the optimal values of f and h can be found by means of alternating minimization (AM), which recursively updates one of the variables while keeping the other variable "frozen" and visa versa. It is important to emphasize, however, that the cost function in (2) is not jointly convex in f and h, even when the regularization functionals φ and ψ are. Consequently, the minimization routine is not guaranteed to converge to a globally optimal solution, in general.

The idea of "hybrid" deconvolution can be used to substantially constrain the space of admissible solutions of (2), thus largely improving one's chances to attain the global optimizer. In particular, let's assume for a moment that the IQ image g is now available along with partial information on the PSF, namely, the magnitude $\hat{\mathbf{h}}$ of its Discrete Fourier Transform (DFT) $\mathcal{F} : h \mapsto \hat{h}$. In this case, the optimization problem (2) can be reformulated in a constrained form as

$$\min_{f,h} \left\{ (1/2) \left\| f * h - g \right\|_F^2 + \varphi(f) \right\}, \quad \text{s.t. } |\mathcal{F}(h)| = \hat{\mathbf{h}}. \tag{3}$$

As before, this optimization problem can be solved by means of AM, which will alternate between sequential updates of f and h according to

$$f \leftarrow \arg\min_{f} \left\{ (1/2) \left\| f * h - g \right\|_F^2 + \varphi(f) \right\}, \tag{4}$$

$$h \leftarrow \arg\min_{h} \left\| f * h - g \right\|_F^2, \ \text{s.t.} \ |\mathcal{F}(h)| = \hat{\mathbf{h}}. \tag{5}$$

Assuming the functional φ to be convex, problem (4) admits an efficient solution in terms of its associated proximal operator defined as

$$\text{prox}_{\varphi}(y) = \arg\inf_{x} \left\{ (1/2) \|y - x\|_F^2 + \varphi(x) \right\}. \tag{6}$$

Thus, for example, a global minimizer of (4) can be obtained as the stationary point of iterations produced by the proximal gradient method (PGM) according to [8]

$$f^{t+1} = \text{prox}_{\varphi} \left(f^t + \bar{h} * (g - f^t * h) \right), \tag{7}$$

with $\bar{h}[n, m] = h^*[-n, -m]$ and assuming h to be normalized so that $\|\hat{h}\|_\infty \leq 1$, with $\hat{h} = \mathcal{F}(h)$. Moreover, there exist several ways to significantly increase the rate of convergence of PGM, which makes it a particularly favourable choice in practical computations [8].

The second update given by (5) requires a less traditional approach. To solve this problem efficiently, we use Parseval's theorem to reformulating it in terms of minimization with respect to the DFT $\hat{h}$ of h, leading to

$$\min_{\hat{h}} \left\| \hat{f} \cdot \hat{h} - \hat{g} \right\|_F^2, \ \text{s.t.} \ |\hat{h}| = \hat{\mathbf{h}}, \tag{8}$$

with the $\cdot$ symbol denoting element-wise multiplication. In addition, the fact that $\hat{h} = \hat{\mathbf{h}} \cdot \hat{u}$, with $\hat{u} = \exp(\jmath \measuredangle \hat{h})$, allows

further simplifications, effectively leading to a minimization with respect to $\hat{u}$, i.e.,

$$\min_{\hat{u}} \left\| (\hat{f} \cdot \hat{\mathbf{h}}) \cdot \hat{u} - \hat{g} \right\|_F^2, \tag{9}$$

over the space of all all-pass (AP) filters $\hat{u}$. Consequently, the resulting optimization problem can be interpreted as a *filter design problem* looking for an all-pass filter $\hat{u}$, with its phase response $\measuredangle \hat{u}$ matching as close as possible the DFT phase given by $\measuredangle \hat{g} - \measuredangle \hat{f}$ or, equivalently, by $\measuredangle(\hat{g} \cdot \hat{f}^*)$.

The current arsenal of filter design algorithms is vast. For the purpose of this work, the design procedure of [9] has been found to be especially useful. In what follows, we describe a modified version of this procedure, adapted for processing of complex-valued signals. In particular, let r be an $(N_1 + 1) \times (N_2 + 1)$ array of complex numbers and let $\hat{r}^{\mathcal{Z}}(z_1, z_2)$ be a two-dimensional z-transform defined by

$$\hat{r}^{\mathcal{Z}}(z_1, z_2) = \sum_{n_1=0}^{N_1} \sum_{n_2=0}^{N_2} r_{n_1,n_2}\, z_1^{-1} z_2^{-1}. \tag{10}$$

It can then be easily verified that

$$\hat{u}^{\mathcal{Z}}(z_1, z_2) = \frac{z_1^{-N_1} z_2^{-N_2}\, \hat{r}^{\mathcal{Z}}(z_1^{-1}, z_2^{-1})}{\hat{r}^{\mathcal{Z}}(z_1, z_2)} \tag{11}$$

defines the transfer function of an AP system of order L, with $L = \max\{N_1, N_2\}$. Furthermore, restricting (z_1, z_2) to the unit sphere (thus reducing $\hat{r}^{\mathcal{Z}}(z_1, z_2)$ and $\hat{u}^{\mathcal{Z}}(z_1, z_2)$ to their associated DFTs $\hat{r}(\omega_1, \omega_2)$ and $\hat{u}(\omega_1, \omega_2)$) suggests that the phases of $\hat{r}$ and $\hat{u}$ are related according to

$$\measuredangle \hat{r}(\omega_1, \omega_2) = -(1/2)\big(N_1\omega_1 + N_2\omega_2 + \measuredangle \hat{u}(\omega_1, \omega_2)\big), \tag{12}$$

thereby making it possible to design the AP filter $\hat{u}$ in terms of $\hat{r}$. Specifically, denoting by $r^{\Re}$ and $r^{\Im}$ the real and imaginary parts of r, respectively, it is straightforward to verify that (10) suggests that

$$\sum_{n_1=0}^{N_1} \sum_{n_2=0}^{N_2} r^{\Re}_{n_1,n_2} \mathcal{S}^{\measuredangle \hat{r}}_{n_1,n_2}(\omega_1, \omega_2) + r^{\Im}_{n_1,n_2} \mathcal{C}^{\measuredangle \hat{r}}_{n_1,n_2}(\omega_1, \omega_2) = 0, \tag{13}$$

with $\mathcal{S}^{\measuredangle \hat{r}}_{n_1,n_2}(\omega_1, \omega_2) = \sin(\omega_1 n_1 + \omega_2 n_2 + \measuredangle \hat{r}(\omega_1, \omega_2))$ and $\mathcal{C}^{\measuredangle \hat{r}}_{n_1,n_2}(\omega_1, \omega_2) = -\cos(\omega_1 n_1 + \omega_2 n_2 + \measuredangle \hat{r}(\omega_1, \omega_2))$. The above equation can be expressed in a more compact form by stacking the vectorized versions of $r^{\Re}$ and $r^{\Im}$ into a column vector $\mathbf{r} = [\mathrm{vec}(r^{\Re})^T, \mathrm{vec}(r^{\Im})^T]^T$, while letting $\mathbf{A}(\omega_1, \omega_2)$ be a row vector of function-valued components defined by the basis functions $\mathcal{S}^{\measuredangle \hat{r}}_{n_1,n_2}(\omega_1, \omega_2)$ and $\mathcal{C}^{\measuredangle \hat{r}}_{n_1,n_2}(\omega_1, \omega_2)$, arranged in congruence with the order of the elements of $\mathbf{r}$. Then, in the new notations, (13) becomes

$$\mathbf{A}(\omega_1, \omega_2)\, \mathbf{r} = 0, \quad \forall (\omega_1, \omega_2). \tag{14}$$

In practice, $\measuredangle \hat{r}(\omega_1, \omega_2)$ is computed using (12), upon replacing $\measuredangle \hat{u}(\omega_1, \omega_2)$ with the desired phase response, i.e., $\measuredangle(\hat{g} \cdot \hat{f}^*)$. The latter is usually too noisy to be modelled with reasonably small values of L, which makes the equality in (14) practically unattainable. It is nevertheless possible, however, to solve the equation in a least-square sense by first computing a matrix $\mathbf{R}$ according to

$$\mathbf{R} = \int_{-\pi}^{\pi} \int_{-\pi}^{\pi} \mathbf{A}(\omega_1, \omega_2)^T \mathbf{A}(\omega_1, \omega_2)\, d\omega_1 d\omega_2, \tag{15}$$

and then minimizing $\mathbf{r}^T \mathbf{R}\, \mathbf{r}$ subject to energy normalization $\|\mathbf{r}\|^2 = 1$. By the well-known Rayleigh's principle, this problem is solved by the eigenvector of $\mathbf{R}$ corresponding to the smallest eigenvalue of the matrix.

Once available, the optimal $\mathbf{r}$ can be reshaped into a complex array $\hat{r}$ to compute the phase of the AP filter $\hat{u}$, which can, in turn, be used to compute an updated value of the PSF as $h = \mathcal{F}^{-1}(\hat{\mathbf{h}} \cdot \hat{u})$. Subsequently, the latter can be passed back into (4), commencing a new cycle of the AM procedure. It has been observed that up to five iterations of AM initiated with $\hat{h} = \hat{\mathbf{h}}$ are usually sufficient for its convergence.

3. EXPERIMENTAL RESULTS

3.1. Additional assumptions

Before presenting the experimental results, the nature of the regularization functional φ in (3) needs to be specified. Usually, φ is chosen to reflect one's *a priori* beliefs on the statistical behaviour of tissue reflectivity, which, in turn, depends on the echogenicity of insonified tissue. For instance, diffuse scattering is conventionally associated with Gaussian statistics, in which case setting $\varphi(f) = \|f\|_F^2$ would be an apt choice. On the other hand, the behaviour of specular reflections adheres more naturally to Laplacian statistics, leading to $\varphi(f) = \|f\|_1$. Practical sonograms, however, can rarely be described exclusively by one of these two statistical models. In this case, the Huber model [10] have been observed to be a propitious "middle round", allowing characterization of complex echogenicity patterns based on a single stochastic model. The Huber regularization suggests φ to be defined as

$$\varphi(f) = \gamma \sum_{n=0}^{N-1} \sum_{m=0}^{M-1} \begin{cases} |f_{n,m}|^2, & |f_{n,m}| \le a \\ 2a|f_{n,m}| - a^2, & |f_{n,m}| > a \end{cases}, \tag{16}$$

where $\gamma > 0$ is a user-defined regularization parameter, while $a > 0$ sets a dividing line between a Gaussian and Laplacian behaviour of the values of tissue reflectivity. In this work, we used $\gamma = 0.002$ and $a = 0.05$.

The final missing piece in the description of the proposed method is the estimation of $\hat{\mathbf{h}}$. Fortunately, an accurate estimate of $\hat{\mathbf{h}}$ is easy to find by means of homomorphic denoising of [5], which was used in the current work as well.

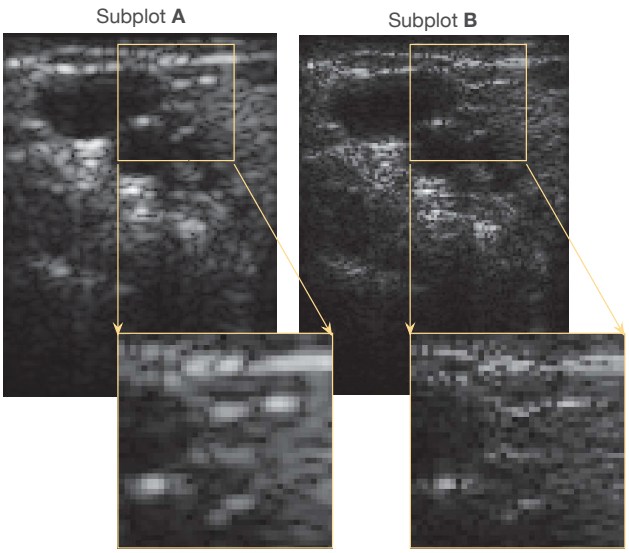

Fig. 1. Subplot (A): Original image, Subplot (B) Reconstruction by means of the proposed algorithm.

3.2. Reconstruction of in vivo scans

The proposed blind deconvolution method has been tested using *in vivo* data acquired from healthy volunteers using a Siemens Sonoline Antares$^{\text{TM}}$ scanner equipped with the Axius Direct Ultrasound Research Interface (URI). The acquired RF images were subjected to a standard demodulation procedure, followed by antialiasing filter and downsampling so that the effective sampling rate of the resulting IQ images was approximately equal to twice its critical value (in both the axial and lateral directions). Subplot A of Fig. 1 depicts a segment of a typical abdominal image from the experimental dataset. Note that the chosen image is characterized by a range of diverse features, including both specular reflection and diffuse scattering.

Subplot B of Fig. 1, on the other hand, shows the same image after the application of the proposed deconvolution algorithm. To obtain this result, a total number of AM iterations was set to five, with $N_1 = N_2 = 3$. It deserves noting that the whole reconstruction procedure (including the deconvolution of the 4480×384 RF image, filtering, estimation of $\hat{\mathbf{h}}$, and the AM iterations) took only 0.55 sec on a standard 2.6 GHz Intel Core i7 via straightforward MATLAB implementation without GPU acceleration. Hence, the computational efficiency of the proposed method can be regarded as reasonable.

One can see that the procedure of blind deconvolution results in a noticeable increase in spatial image resolution and improved contrast. Moreover, the proposed method seems to produce neither "clipping" nor Gibbs-like artifacts typical for ℓ_1- and ℓ_2-norm regularizations, respectively. The absence of "ringing" effects and residual blur around sharp image details is likely to indicate proper recovery of the PSF phase.

4. CONCLUSIONS

In this paper, a novel approach to the problem of blind deconvolution of medical ultrasound images has been proposed. In its core, the method belongs to the family of "hybrid" deconvolution techniques, which estimate tissue reflectivity based on only partial information on the PSF, and, in particular, its power spectrum. As opposed to earlier works in the same direction, the proposed method relies on an implicit formulation, which allows recovering the spectral information beyond the transducer passband. The results obtained in a preliminary experimental study indicate a promising potential of the method, thus warranting its further development and testing.

5. REFERENCES

[1] C. Dalitz, R. Pohle-Fröhlich, and T. Michalk, "Point spread functions and deconvolution of ultrasonic images," *IEEE Trans. Ultrason. Ferroelectr. Freq. Control*, vol. 62, no. 3, pp. 531–544, 2015.

[2] R. G. Newton, *Scattering Theory of Waves and Particles*, Dover Publications, 2002.

[3] M. Florea, A. Basarab, D. Kouamé, and S. Vorobyov, "An axially variant kernel imaging model applied to ultrasound image reconstruction," *IEEE Signal Process. Lett.*, vol. 25, no. 7, pp. 961–965, 2018.

[4] T. Taxt, "Restoration of medical ultrasound images using two-dimensional homomorphic deconvolution," *IEEE Trans. Ultrason. Ferroelectr. Freq. Control*, vol. 42, no. 4, pp. 543–554, 1995.

[5] O. Michailovich and D. Adam, "A novel approach to the 2-D blind deconvolution problem in medical ultrasound," *IEEE Trans. Med. Imag.*, vol. 24, no. 1, pp. 86–104, 2005.

[6] C. Yu, C. Zhang, and l. Xie, "A blind deconvolution approach to ultrasound imaging," *IEEE Trans. Ultrason. Ferroelectr. Freq. Control*, vol. 59, no. 2, pp. 271–280, 2012.

[7] O. Michailovich and A. Tannenbaum, "Blind deconvolution of medical ultrasound images: A parametric inverse filtering approach," *IEEE Trans. Image Process.*, vol. 16, no. 12, pp. 3005–3019, 2007.

[8] A. Beck and M. Teboulle, "A fast iterative shrinkage-thresholding algorithm for linear inverse problems," *SIAM J. Imaging Science*, vol. 2, pp. 183–202, 2009.

[9] S.-C. Pei and J.-J. Shyu, "Eigenfilter design of 1-D and 2-D IIR digital all-pass filters," *IEEE Trans. Signal Process.*, vol. 42, no. 4, pp. 966–868, 1994.

[10] P. J. Huber, *Robust statistics*, John Wiley & Sons, 1981.